Optics Letters

Improving laser damage resistance of 355 nm high-reflective coatings by co-evaporated interfaces

Huanbin Xing,[1,2] Meiping Zhu,[1,*] Yingjie Chai,[1,2,3] Kui Yi,[1] Jian Sun,[1] Yun Cui,[1] and Jianda Shao[1]

[1]Key Laboratory of Materials for High Power Laser, Shanghai Institute of Optics and Fine Mechanics, No. 390 Qinghe Road, Jiading District, Shanghai, China
[2]Graduate School of Chinese Academy of Sciences, Beijing, China
[3]e-mail: chaiyingjie1990@siom.ac.cn
*Corresponding author: bree@siom.ac.cn

Received 11 January 2016; revised 2 February 2016; accepted 9 February 2016; posted 10 February 2016 (Doc. ID 257190); published 14 March 2016

355 nm high-reflective multilayer coatings with or without coevaporated interfaces (CEIs) were prepared by electron beam evaporation under the same deposition condition. Their transmission spectra, surface roughness, and mechanical stress properties were evaluated. Elemental composition analysis of the multilayer interfaces was performed using x-ray photoelectron spectroscopy, and laser-induced damage thresholds were obtained in both 1-on-1 and 300-on-1 testing modes. The coatings with CEIs reveal a lower mechanical stress and a higher laser damage resistance when irradiated with high laser fluence, and the corresponding damage modeling indicates that CEIs can significantly decrease defect density. The resulting damage morphologies show that CEI coatings can significantly suppress coating delamination and exhibit a "bulk-like" damage behavior, demonstrating better damage performance against high-power lasers.

OCIS codes: (140.3330) Laser damage; (310.6870) Thin films, other properties; (140.3440) Laser-induced breakdown.

http://dx.doi.org/10.1364/OL.41.001253

Multilayer dielectric coatings fabricated by e-beam (EB) evaporation are widely used in laser systems because of their fine optical qualities and high laser damage resistance. For example, high laser damage threshold multilayer coatings manufactured by EB were utilized in the National Ignition Facility (NIF), Shenguang (SG III) [1], and other places. However, great effort is still underway to achieve a higher laser damage resistance of multilayer coatings in recent years [2–6]. In the nanosecond regime, damage can be attributed to different kinds of defects [7]. The interface between two materials is considered one of the main damage sources due to the interfacial absorption [8], high density of defects [9], and significant differences between thermal expansion coefficients of the evaporated materials [10]. The interfacial issues may lead to severe coating delamination and flat bottom pits [11] when irradiated by high-power laser pulses. Previous studies demonstrated that delamination could be suppressed by introducing a thicker SiO_2 overcoat layer [12] or by using a double-stack multilayer design [13], thus improving the laser damage resistance of a coating. However, when the fluence of laser irradiation increases, interfaces inevitably become one of the damage sources. The discrete interface problem is one of the topics to be solved in the field of high-power laser coatings. In recent years, researchers have proposed applying mixtures by coevaporation or cosputtering processes in both monolayers and multilayers [14]. Here, the coevaporation processes were used at interfaces in conventional (CON) EB coatings.

In this Letter, we mainly focus on the impact of multilayer interfaces on the 355 nm high-reflective (HR) coatings. With the coevaporation process at the interfaces, multilayer coatings with special interfaces were prepared. Mechanical stress characteristics and interface elemental composition profiles for the coatings with or without coevaporation interfaces (CEIs) were acquired. The effect of CEIs on the laser damage resistance of the coatings was evaluated by studying their laser-induced damage performances in both 1-on-1 and 300-on-1 testing modes.

In this experiment, two kinds of dielectric multilayer coatings were prepared using a Leybold coater: CON and CEI coatings, respectively. The coating designs were both Sub/$12L(HL)^8(ML)^{10}$ M12.2L/A, where "Sub" denotes substrate, "A" denotes the air, and "H", "M", and "L" denote HfO_2, Al_2O_3, and SiO_2, respectively. The coatings had high reflectivity for 355 nm at an incidence angle of 45° with S-polarization designed by commercial Essential Macleod. All the H, L, and M layers had quarter-wave optical thicknesses (QWOT) corresponding to the reference wavelength of 386 nm. As shown in Fig. 1, during CON processes, a shutter was applied to guarantee only one source evaporation for each layer. However, for CEI processes, the shutter was not used, and the CEIs were achieved by precisely controlling the evaporation rates of two materials during the coevaporation period. The CEI physical thicknesses were maintained at a value of about 10 nm by controlling the duration of the coevaporation process. A commercial optical monitoring system OMS 3000 (Leybold Optics

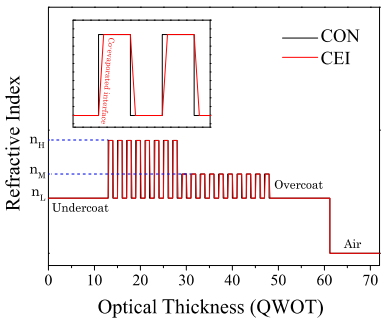

Fig. 1. Refractive index profiles for the CON and CEI coatings. The CEI multilayer coating interface was by coevaporation, and its optical thickness coincides with that of the CON coating during the HL (HfO_2/SiO_2) and ML (Al_2O_3/SiO_2) deposition cycles.

GmbH) was used for each layer to ensure the same total optical thickness during deposition. The coatings were deposited by using Hf [10], Al_2O_3, and SiO_2 as the starting materials. All the K9 substrates were supersonically cleaned before clamping, and ion-assisted cleaned in the coating chamber before deposition. The chamber was pumped to a base pressure of 4.5×10^{-4} Pa, and the substrates were baked to 473 K prior to deposition. The deposition rates for the HfO_2, Al_2O_3, and SiO_2 layers were 0.11 nm/s, 0.15 nm/s, and 0.26 nm/s, and the corresponding oxygen pressures in the vacuum chamber were 1.4×10^{-2} Pa, 1.3×10^{-2} Pa, and 5.5×10^{-2} Pa, respectively. The transmission of both samples (45°, S-polarization) measured by a spectrometer (Lambda 1050 UV/VIS/NIR, Perkin-Elmer) were lower than 0.1% at 355 nm (Fig. 2).

Surface roughness of both coatings were evaluated by an atomic force microscopy (AFM), and the obtained root mean square (RMS) roughness values for the CON and CEI coatings were 1.679 nm and 1.627 nm, respectively, which could be regarded as a small difference between both samples. Mechanical properties of the multilayer coatings were characterized by a ZYGO Mark III-GPI interferometer at a wavelength of 632.8 nm. Substrate radii before (R_1) and after (R_2) deposition were used to calculate their total stress (σ_{tot}) utilizing Stoney's equation [15]:

$$\sigma_{tot} = \frac{E_s}{6(1-\nu_s)} \cdot \frac{t_s^2}{t_f} \cdot \left(\frac{1}{R_2} - \frac{1}{R_1}\right). \quad (1)$$

Here E_s and ν_s denote the Young's modulus and Poisson ratio of the substrate, while t_s and t_f represent the thicknesses of the substrate and the film, respectively. As shown in Table 1, the CEI samples have lower mechanical stress than the CON samples, indicating that CEIs are capable of releasing coatings stress. The

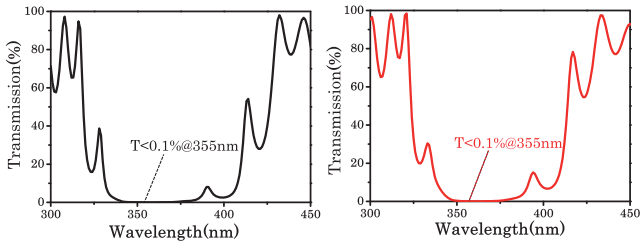

Fig. 2. Transmittance spectra for the (a) CON and (b) CEI coatings. In both cases, the transmittance values for S-polarized light were lower than 0.1% at a wavelength of 355 nm and incident angle of 45°.

Table 1. Mechanical Stress Values for the CON and CEI Coatings as Functions of Time[a]

Time (days)	CON (MPa)	CEIs (MPa)
10	−88.80 ± 6.10	−61.01 ± 4.19
120	−79.70 ± 5.48	−58.80 ± 4.04
150	−73.88 ± 5.07	−56.73 ± 3.90

[a]All the coating stress was compressive and shown in the negative. All the tests were conducted at a relative humidity of 45 ± 5% and temperature of 22 ± 2°C.

subsequent measurements for both coatings showed a gradual mechanical stress relief with time.

Sample interface elemental composition profiles were characterized by a K-Alpha x-ray photoelectron spectrometer (XPS) in a high vacuum environment with a base pressure of less than 1×10^{-7} Pa. The spectrometer was equipped with the monochromatic Al K-alpha ($h\nu = 1486.6$ eV) x-ray radiation as the excitation source. The charging compensation was applied, assuming that the C 1s peak appeared at a binding energy of 285 eV. Depth profile measurements were conducted using 1 keV Ar^+ ions with an ion current of 3 mA and a spot size diameter of 400 μm. The etching rates were equal to 0.16 nm/s and 0.07 nm/s for SiO_2 and Al_2O_3, respectively. The commercial Avantage software with tabulated XPS standard data was used to analyze the obtained data. An analysis of the XPS spectra was carried out after Shirley background subtraction. The XPS peak positions (Si 2p, Al 2p, and O 1s) for both samples were not apparently affected by the presence of CEIs, indicating the absence of new compounds at the interfaces. According to Fig. 3, the XPS results reveal the existence of a pure deposited material and diffused species in each layer due to the diffusion between neighboring layers in EB multilayer coatings. In order to determine the physical thicknesses of the CEIs, elemental compositions of the two samples were characterized by the same etching process, and elemental composition changing should be considered. The etching time for the pure Al_2O_3 layer (with the SiO_2 content equal to 0%) of the CEI coatings was about 100 s shorter than that for the CON coating, indicating that the thickness of the CEI was about 7 nm, which is close to the originally set value. The adhesion property of the adjacent materials can be further improved by CEIs.

The laser damage system utilized in this work was described in detail elsewhere [16]. Laser damage experiments were carried

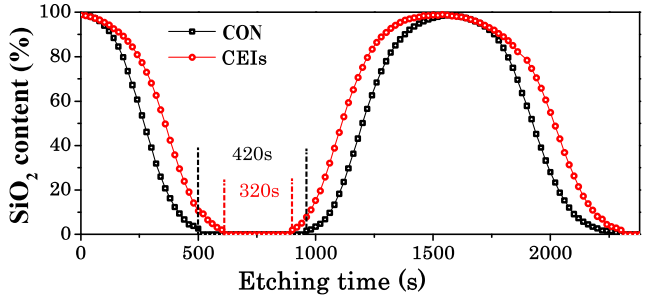

Fig. 3. SiO_2 fractions as functions of etching time for the ML (Al_2O_3/SiO_2) layers in the CON and CEI coatings. The dots denote the experimental data. The pure Al_2O_3 etching duration for the CEI coating is 100 s shorter than that for the CON coating.

out using 8 ns pulses with S-polarization from a 355 nm Nd: YAG laser at a 45° incidence angle. Laser-induced damage threshold (LIDT) tests were performed in the 1-on-1 and 300-on-1 modes, according to the ISO 21254 standard procedure [17]. Due to the uncertainties caused by the differences between samples (3%), measurements of the laser spot area (5%), and fluctuations of laser energy (5%), the relative error of the damage probability measurements amounts to ±15%. Both single-shot and multiple-shot laser tests were conducted to investigate the laser damage performance and safe operating lifetimes of the multilayer coatings [18]. A visible He–Ne laser was used as the illumination source [16]. The e^{-2} spot diameters along the x and y axes measured by a knife-edge method were 380 μm and 460 μm, respectively. Damage was evaluated by comparing the test areas before and after laser irradiation. The site spacing was as great as 1.5 mm, about 3 times larger than the laser spot diameter, to prevent the influence of the neighboring damage. Twenty sites were probed for each obtained energy fluence value. The LIDT was defined as the energy fluence of an incident pulse corresponding to the damage probability of 0%. Damage morphologies were characterized by a scanning electron microscope (SEM, Carl Zeiss AURIGA), operating at an accelerating voltage of 1 kV. A step profiler with a 2 μm pinhead radius was also used for mapping damage depth in the 300-on-1 mode.

The 355 nm laser damage was mainly induced by nanoabsorbing defects. As shown in Fig. 4, the LIDTs of the CEI coatings were slightly improved by CEIs. However, the CEI coatings exhibit a better laser damage resistance in both 1-on-1 and 300-on-1 modes when irradiated by lasers with higher fluence (especially at fluence values greater than 10 J/cm^2). The defect thresholds and densities (related to shapes and slopes of the damage probability curves) were determined from the 1-on-1 and 300-on-1 laser damage testing data by using the model developed by Krol *et al.* [7], which assumes Gaussian distribution of defect thresholds, and the energy mostly deposits on the

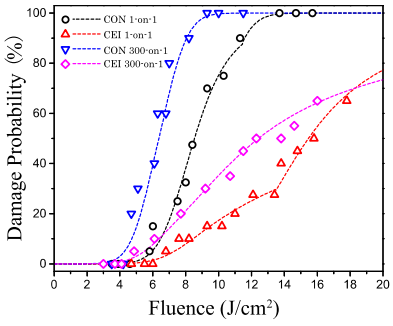

Fig. 4. Damage probability curves for the CON and CEI coatings obtained in the 1-on-1 and 300-on-1 modes. The dots denote the experimental data, and the dashed lines denote the fitted curves.

defects when laser-induced damage occurs. The function depends on three parameters: defect density d_i, defect damage-threshold mean value T_i, and threshold standard deviation ΔT_i,. The parameters extracted from the best-fit curves are listed in Table 2 and the existence of two kinds of defects in both samples is noted. The low-threshold defect and the high-threshold defect show: T_1(CON 1-ON-1) ≈T_1(CEIs 1-ON-1), T_2(CON 1-ON-1) ≈T_2(CEIs 1-ON-1), which indicated defect types are not radically changed. For 355 nm single-nanosecond pulse irradiations, both defects in the coating layers and at the interfaces could induce damage. Although the defect threshold values T_1 (1-on-1) and T_2 (1-on-1) were not apparently improved, the defect densities d_1(CEIs 1-on-1) and d_2 (CON 1-on-1) were much lower than those of CON coatings, indicating that both defect densities were reduced. The decrease in volume density was due to the smaller physical thickness of the pure material (measured by XPS) [19]. For defects at the interfaces, CON coatings with discrete interfaces may introduce more defects because of the alternative evaporation processes of the two different materials. In addition, both coatings show that T_1 (1-on-1) > T_1 (300-on-1) and T_2 (1-on-1) > T_2 (300-on-1) due to the fatigue effects of the multilayer coatings under multishot irradiation and fluctuations of laser fluence [20].

As shown in Fig. 5, the 1-on-1 laser damage morphology studies reveal that the CON coatings exhibit surface delamination induced by several absorption defects in the center (in particular, when irradiated by high-power lasers). However, the CEI coatings exhibit a "bulk-like" damage behavior [21] when irradiated by lasers with low fluence. The bulk-like damage morphologies are mainly induced by absorption defects in the damage centers with slightly cracked extensions in the radial direction. Damage morphologies characterized by severe delamination and flat pits were hardly observed for the CEI coatings, which may be due to the adhesion strength enhancement offered by CEIs. Besides, the damage pit sizes of CEI coatings are obviously smaller than those of CON coatings (see Fig. 5). The improvement of 1-on-1 laser damage performance was due to the lower mechanical stress in interface-modified coatings, which could effectively suppress delamination and damage development. For 300-on-1 laser irradiation, the damage morphologies of CON and CEI coatings are very much alike, except that the damage sizes of CEI coatings are smaller and shallower than those of CON coatings when irradiated by same laser fluence (see Fig. 6). For example, when the CON/CEI coatings was irradiated by laser fluence of 10.7 J/cm^2, we got the average size of craters of 3.85 μm width and 0.33 mm depth for CON samples, 2.91 μm width and 0.22 mm depth for CEI samples.

In conclusion, 355-nm HR coatings with/without CEIs were prepared, and their optical and mechanical properties were evaluated. The damage performances of the two samples were compared both in the 1-on-1 and 300-on-1 modes. The CEI

Table 2. Defect Parameters Extracted from the Best-Fit Curves

	d_1 (1/mm^2)	T_1 (J/cm^2)	ΔT_1 (J/cm^2)	d_2 (1/mm^2)	T_2 (J/cm^2)	ΔT_2 (J/cm^2)
$Con_{1\text{-on-1}}$	46.8	7.0	2.7	251.2	11.5	4.1
$Con_{300\text{-on-1}}$	51.0	6.0	2.3	250.8	8.6	4.1
$CEIs_{1\text{-on-1}}$	4.9	7.2	2.7	28.0	12.6	4.0
$CEIs_{300\text{-on-1}}$	6.1	5.9	2.5	12.1	7.9	5.1

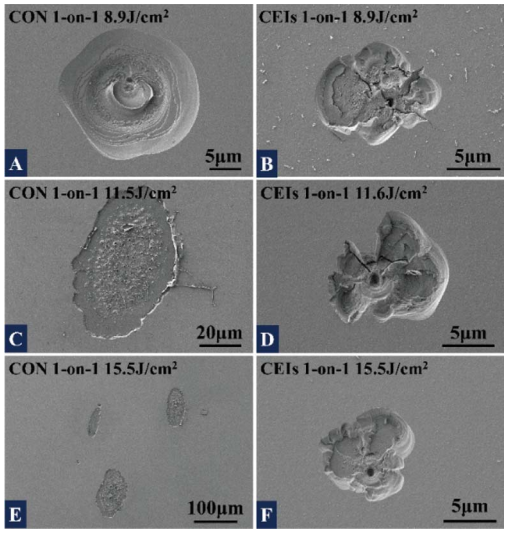

Fig. 5. Damage morphologies for the CON and CEI coatings measured in the 1-on-1 mode with low (A and B), medium (C and D), and high (E and F) laser fluence.

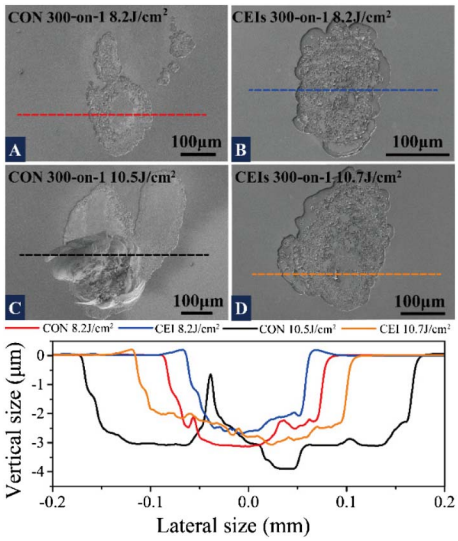

Fig. 6. Damage morphologies for the CON and CEI coatings measured in the 300-on-1 mode with low (A and B) and high (C and D) laser fluence. Depth information (E) for both the CON and CEI samples was obtained by the step profiler, characterizing the maximum depth at the positions marked by the dashed color lines.

coatings reveal a higher laser damage resistance when irradiated with high laser fluence, and the corresponding damage modeling indicates that CEIs can significantly decrease defect density. The damage morphologies obtained for the CEI coatings in the 1-on-1 mode exhibit a bulk-like damage behavior with less delamination and flat bottom pits. The 300-on-1 laser damage mode results in smaller and shallower damage morphologies for the CEI coatings, pointing to their ability to suppress damage growth. By the novelty of introducing the coevaporated process in 355 nm EB coatings, the multilayer interface properties were significantly improved, which can eventually help researchers release the coating mechanical stress and improve the damage resistance of optical coatings to high-power laser fluence.

Funding. Youth Innovation Promotion Association of the Chinese Academy of Sciences; National Natural Science Foundation of China (NSFC) (61505227,61405225).

Acknowledgment. The authors would like to express their gratitude to Prof. Zhengxiu Fan and Hu Wang. The authors would like to acknowledge Dawei Li and Xiaofeng Liu in the LIDT test.

REFERENCES

1. D. X. Hu, J. Dong, D. P. Xu, X. X. Huang, W. Zhou, X. C. Tian, D. D. Zhou, H. W. Guo, W. Zhong, X. W. Deng, Q. H. Zhu, and W. G. Zheng, Chin. Opt. Lett **13**, 041406 (2015).
2. Y. J. Chai, M. P. Zhu, K. Yi, W. L. Zhang, H. Wang, Z. Fang, Z. Y. Bai, Y. Cui, and J. D. Shao, Opt. Lett. **40**, 3731 (2015).
3. Y. J. Chai, M. P. Zhu, Z. Y. Bai, K. Yi, H. Wang, Y. Cui, and J. D. Shao, Opt. Lett. **40**, 1330 (2015).
4. X. F. Liu, Y. A. Zhao, Y. Q. Gao, D. W. Li, G. H. Hu, M. P. Zhu, Z. X. Fan, and J. D. Shao, Appl. Opt. **52**, 2194 (2013).
5. W. W. Liu, C. Y. Wei, S. L. Chen, Z. Fang, K. Yi, and J. D. Shao, Opt. Commun. **301-302**, 12 (2013).
6. Z. K. Yu, H. B. He, W. Sun, H. J. Qi, M. H. Yang, Q. L. Xiao, and M. P. Zhu, Opt. Lett. **38**, 4308 (2013).
7. H. Krol, L. Gallais, C. Grèzes-Besset, J.-Y. Natoli, and M. Commandré, Opt. Commun. **256**, 184 (2005).
8. P. A. Temple, Appl. Phys. Lett. **34**, 677 (1979).
9. S. C. Weakley, C. J. Stolz, Z. L. Wu, R. P. Bevis, and M. K. von Gunten, Proc. SPIE **3578**, 137 (1998).
10. C. J. Stolz, F. Y. Génin, T. A. Reitter, and N. Molau, Proc. SPIE **2966**, 265 (1997).
11. C. J. Stolz, L. M. Sheehan, M. K. Gunten, R. P. Bevis, and D. Smith, Proc. SPIE **3738**, 318 (1999).
12. M. P. Zhu, K. Yi, D. W. Li, X. F. Liu, H. J. Qi, and J. D. Shao, Opt. Commun. **319**, 75 (2014).
13. H. Yu, L. Q. Wu, C. F. Liu, J. D. Shao, and Z. X. Fan, Opt. Laser Technol. **44**, 810 (2012).
14. M. Mende, L. O. Jensen, H. Ehlers, W. Riggers, H. Blaschke, and D. Ristau, Proc. SPIE **8168**, 816821 (2011).
15. X. Li, W. L. Zhang, J. Sun, J. Liu, Y. Q. Hou, L. Lin, K. He, and K. Yi, Appl. Sur. Sci. **282**, 226 (2013).
16. W. W. Liu, C. Y. Wei, J. B. Wu, H. Cui, K. Yi, and J. D. Shao, Opt. Express **21**, 22476 (2013).
17. "Lasers and laser-related equipment–test methods for laser-induced damage threshold," Part 1 (ISO 21254-1:2011) and Part 2 (ISO 21254–2:2011) (International Organization for Standardization, 2011).
18. J.-Y. Natoli, B. Bertussi, and M. Commandré, Opt. Lett. **30**, 1315 (2005).
19. J.-Y. Natoli, L. Gallais, H. Akhouayri, and C. Amra, Appl. Opt. **41**, 3156 (2002).
20. W. W. Liu, C. Y. Wei, K. Yi, and J. D. Shao, Chin. Opt. Lett. **13**, 091404 (2015).
21. R. N. Raman, R. A. Negres, M. J. Matthews, and C. W. Carr, Opt. Mater. Express **3**, 765 (2013).